

# Old Phase Remnants in First Order Phase Transitions

Philip Lu,<sup>1,\*</sup> Kiyoharu Kawana,<sup>1,†</sup> and Ke-Pan Xie<sup>2,‡</sup>

<sup>1</sup>Center for Theoretical Physics, Department of Physics and Astronomy, Seoul National University, Seoul 08826, Korea

<sup>2</sup>Department of Physics and Astronomy, University of Nebraska, Lincoln, NE 68588, USA

First order phase transitions (FOPTs) are usually described by the nucleation and expansion of new phase bubbles in the old phase background. While the dynamics of new phase bubbles have been extensively studied, a comprehensive treatment of the shrinking old phase remnants remained undeveloped. We present a novel formalism for remnant statistics in FOPTs and perform the first analytical calculations of their distribution. By shifting to the reverse time description, we identify the shrinking remnants with expanding old phase bubbles, allowing a quantitative evolution and determination of the population statistics. Our results not only provide essential input for cosmological FOPT-induced soliton/primordial black hole formation scenarios, but can also be readily applied to generic FOPTs.

**Introduction**– First order phase transitions (FOPTs) are found across disciplines as diverse as biology [1, 2], condensed matter physics [3, 4], and cosmology [5]. In the cosmological context, FOPTs are a natural consequence of many Beyond Standard Model theories, and could play a crucial role in generating the matter-antimatter asymmetry [6–10], forming dark matter [11–21] and primordial black holes (PBHs) [22–41], and leave detectable signals in current or near-future gravitational wave detectors [42–47].

Cosmological FOPTs happen through the nucleation and growth of new true vacuum (TV) phase bubbles in the old false vacuum (FV) phase background. More attention has been focused on the calculation and estimation of the properties of TV bubbles, whose statistics are relevant for electroweak baryogenesis [6–10], inflationary models, and for the production of gravitational waves [48–50]. As a result, analytic methods were developed to estimate the TV nucleation rate, wall velocity, and bubble distribution [51–63]. On the other hand, FV remnants are more relevant for the mechanisms involving trapping particles in the FV to realize baryogenesis [64], dark matter [14–21] and PBHs [32–36]. Lacking an equivalent detailed description of the FV remnants, previous studies had to either use naive estimations of the average remnant size and density [15, 19], or take those observables as free parameters [32, 33].

In this *Letter*, we develop a method for calculating remnant statistics from first principles. In the existing framework, the FV phase acquires a decay probability to the energetically favorable TV phase below the critical temperature. The vacuum pressure causes the TV bubbles to expand, filling up the space and leaving shrinking pockets of disconnected FV remnants (as illustrated in Fig. 1). We extend the TV bubble nucleation formalism to include FV bubble nucleation by considering the phase transition in reverse. From this reverse time description, the centers of the collapsing remnants with time flowing forward can be viewed as the nucleation sites of FV bubbles with time flowing

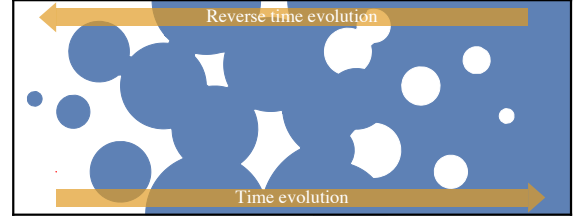


FIG. 1. Progression of the FOPT: with the flow of time from left to right, the initial FV (white) space is nucleated with TV (blue) bubbles, which populate and surround the shrinking FV bubbles. In the reversed time description, FV bubbles nucleate and grow in a TV dominated space, eventually resulting in shrinking TV bubbles.

backwards. Thus, the methods used for TV bubbles can be adapted for the dynamics of FV bubbles. We perform the first calculation of the properties and evolution of the FV bubbles based on the *reverse* time description of the FOPT. Although we present our results within a cosmological context, they can be easily adapted to general FOPTs in fields such as condensed matter physics and biology.

**True vacuum bubbles**– We review the existing TV nucleation formalism for cosmological phase transitions. We assume thin walls and constant velocity  $v_w$  throughout, which is a good approximation for a range of moderately strong FOPTs [57]. Consider a Universe initially in an FV phase at high temperatures. Below the critical temperature  $T_c$ , the TV phase becomes energetically favorable, giving a non-zero probability for the FV space to tunnel to the TV. The TV nucleation rate per unit volume and unit time is [54]

$$\Gamma(t) = A(t)e^{-S(t)}, \quad (1)$$

where  $S(t)$  is the smaller of the two instanton bounce actions  $S_3/T$  [65] and  $S_4$  [66] ( $S_3/T$  is typically smaller [57]).

Assuming the bubbles grow spherically outwards, the

radius of a bubble nucleated at time  $t'$  is

$$R(t, t') = v_w \int_{t'}^t dt'' \frac{a(t)}{a(t'')} , \quad (2)$$

where  $a(t)$  is the scale factor of the FLRW metric. The fraction of space in the FV is [52, 53]

$$f_{\text{fv}}(t) = e^{-I(t)} , \quad (3)$$

where

$$I(t) = \int_{t_c}^t dt' \Gamma(t') \frac{a^3(t')}{a^3(t)} \frac{4\pi}{3} R^3(t, t') , \quad (4)$$

with  $t_c$  being the cosmic time corresponding to  $T_c$ . It will be convenient to define the average TV nucleation rate,  $\bar{\Gamma}(t) = f_{\text{fv}}(t)\Gamma(t)$ , which contains a factor of  $f_{\text{fv}}$  since TV bubbles can only nucleate in patches of FV.

The distribution of TV bubbles at time  $t$  with size  $R$  must equal the average nucleation rate at a time  $t'$  at which  $R(t, t') = R$  (when the scale factor is negligible,  $t' = t - R/v_w$ ),

$$\frac{dn_{\text{tv}}}{dR}(t) = \frac{1}{v_w} \bar{\Gamma}(t') \frac{a^4(t')}{a^4(t)} . \quad (5)$$

Integrating this equation, the total bubble number density is given by

$$n_{\text{tv}}(t) = \int_{t_c}^t dt' \bar{\Gamma}(t') \frac{a^3(t')}{a^3(t)} , \quad (6)$$

where we have used Eq. (2).

**False vacuum bubbles**– In the forward evolution of the phase transition, spherical TV bubbles percolate when the FV volume fraction drops below  $f_{\text{fv}} = 0.71$  [67], forming an infinite connected cluster. As  $f_{\text{fv}}$  decreases, FV regions are separated into shrinking remnants. When the process is considered in reverse, FV bubbles nucleate in a TV background, forming an infinite connected cluster above  $f_{\text{fv}} \approx 1 - 0.71 = 0.29$ . This is the reverse time description of the phase transition, in which we identify shrinking remnants forward in time with nucleating bubbles backward in time.

We develop an analogous formalism for FV bubbles in this reverse time description and calculate a FV bubble nucleation rate. To do so, the nucleation point of a FV bubble can be identified as the projected center of a collapsing remnant, with the nucleation rate equal to the collapse rate. In the final stages of collapse, the size of the remnant is much smaller than the radii of the enveloping TV bubbles, so that the collapsing walls can be treated as flat or planar.

The projection interpretation, in which we extrapolate the wall trajectories to the point of collapse, suggests a counterpart to the reverse time description (the

projection interpretation is extensively discussed in the last part of the *Letter*). In the reverse time description, the FV bubbles nucleated at point  $C$  and time  $t' > t$  grow to a size  $R_r(t, t')$  at time  $t$ . In the alternative forward time description, the FV remnants of size  $R_r(t, t')$  at time  $t$  are those which are projected to collapse at point  $C$  and time  $t' > t$ . These two viewpoints are complementary and fundamentally equivalent.

In one spatial dimension, i.e. on a line, it takes two TV walls to close a FV remnant at a point. For a final collapse at time  $t$ , there needs to be nucleation at some time  $t' < t$  a distance  $v_w(t - t')$  away (neglecting scale factors), and another nucleation at a time  $t'' < t'$  at a distance  $v_w(t - t'')$  away and opposite of the first nucleation. Moving to higher dimensions, the only form of collapse with non-vanishing probability in two (three) dimensions is by three (four) walls forming a triangle (tetrahedron).

The probability of FV remnant collapse per unit volume per unit time,  $d^2 P_r / dV dt$ , at a point  $C$  can be found by integrating along the past wall cone (similar to the light cone but with wall velocity  $v_w$ ) and finding the four points of TV nucleation, so that the four resulting walls would meet at point  $C$  and time  $t$ . We order the TV walls by their proximity in time to  $t$ , with wall 1 being the most recently nucleated wall and thereby avoid unnecessary combinatoric factors. The nucleation point of wall 1 is then only constrained to lie on the past wall cone of point  $C$ , but subsequent walls have to obey angular restrictions to form a closed FV remnant. The angular factors become more complicated with higher spatial dimensions, so we first introduce the formalism in two dimensions before developing the three dimensional case.

**Two spatial dimensions**– For simplicity, we omit scale factors in this exposition and restore them in the full three-dimensional expression Eq. (14). In its final stage, the infinitesimal shrinking FV remnant is a triangle collapsing towards its incenter surrounded by three TV walls. The collapse probability per unit area per unit time,  $d^2 P_r / dA dt$  can be found by integrating along the past wall cone of the collapse point  $C$ . The radial and angular integrations can be separated, and the radial part is

$$v_w f_{\text{fv}}(t) \int_{t_c}^t dt_1 v_w(t - t_1) \Gamma(t_1) \int_{t_c}^{t_1} dt_2 v_w(t - t_2) \Gamma(t_2) \\ \times \int_{t_c}^{t_2} dt_3 v_w(t - t_3) \Gamma(t_3) , \quad (7)$$

with the integration times ordered as  $t_c < t_3 < t_2 < t_1 < t$ , corresponding to the nucleation time of each successive wall. The factors of  $\Gamma$  gives the TV nucleation rate of each wall, and the factor of the FV fraction,  $f_{\text{fv}}$ , is required since only FV points are eligible to collapse to

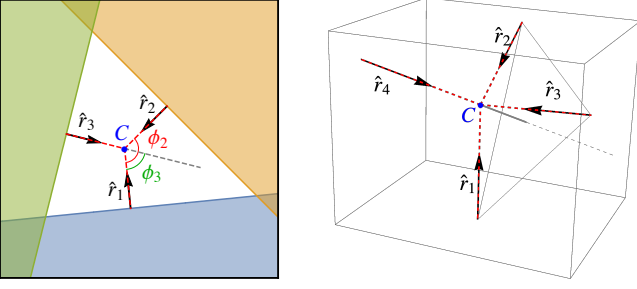


FIG. 2. Geometry of a collapsing FV remnant. **Left:** In 2-dimensional space, to form a closed triangle,  $-\hat{r}_3$  must lie in the angular range bounded by  $\hat{r}_1$  and  $\hat{r}_2$ . **Right:** In 3-dimensional space, to form a closed tetrahedron,  $-\hat{r}_4$  must lie in the solid angle delimited by  $\hat{r}_1$ ,  $\hat{r}_2$  and  $\hat{r}_3$  (the four walls are omitted for clarity).

TV. Since we are integrating along the past wall cone, the integration space is in the FV and no additional factors of  $f_{fv}$  show up inside the integrals. Otherwise, the TV would have already spread to point  $C$  before time  $t$ .

For the angular factor, we denote the normal vector of wall  $i$  by  $\hat{r}_i$ , i.e. the unit vector pointing from the TV nucleation point towards  $C$ . For the three walls to form a closed triangle,  $-\hat{r}_3$  must lie in the angular range bounded by  $\hat{r}_1$  and  $\hat{r}_2$ , as illustrated in the left panel of Fig. 2. To integrate over all the allowed TV bubble configurations, we first choose  $\hat{r}_1$  along the  $\hat{x}$  axis and parameterize the other two normal vectors as

$$\hat{r}_2 = (\cos \phi_2, \sin \phi_2), \quad \hat{r}_3 = (-\cos \phi_3, -\sin \phi_3). \quad (8)$$

Then for  $0 < \phi_2 < \pi$ , the closure of the FV triangle requires  $0 < \phi_3 < \phi_2$ ; while the case  $\pi < \phi_2 < 2\pi$  is just a reflection of the case  $0 < \phi_2 < \pi$  across the  $\hat{x}$  axis. Therefore, the angular integral reads

$$2\pi \int_0^\pi 2d\phi_2 \int_0^{\phi_2} d\phi_3 = 2\pi^3, \quad (9)$$

where the first “ $2\pi$ ” factor represents the integral over the arbitrary  $\hat{r}_1$  angle, while the “2” factor in  $\phi_2$  integral accounts for the  $\pi < \phi_2 < 2\pi$  region.

In the reverse time description, the FV bubble nucleation rate is defined as the remnant collapse probability per unit area per unit time,  $\Gamma_r^{2d}(t) = d^2 P_r / dA dt$ . Combining Eqs. (7) and (9), the FV bubble nucleation rate in two dimensions is

$$\Gamma_r^{2d}(t) = 2\pi^3 v_w^4 f_{fv}(t) \int_{t_c}^t dt_1 (t - t_1) \Gamma(t_1) \times \int_{t_c}^{t_1} dt_2 (t - t_2) \Gamma(t_2) \int_{t_c}^{t_2} dt_3 (t - t_3) \Gamma(t_3). \quad (10)$$

**Three spatial dimensions**— Next we build on our two dimensional results and apply the method to three dimensions. Integrating over the past wall cone, the radial factor is similar, but the angular factor is more complicated, as the three-dimensional remnant is now tetrahedral with four collapsing walls. Ordering the walls temporally and labeling the normal vectors as before, the condition that the four walls form a tetrahedron is that  $-\hat{r}_4$  should lie in the solid angle delimited by  $\hat{r}_1$ ,  $\hat{r}_2$  and  $\hat{r}_3$ , as illustrated in the right panel of Fig. 2.

With the collapse point  $C$  at the origin, we set the  $\hat{z}$  axis in the direction of  $\hat{r}_1$  and  $\hat{y}$  axis along the  $\hat{r}_1 \times \hat{r}_2$  direction, defining our spherical coordinate system. The normal vectors can then be parameterized as

$$\begin{aligned} \hat{r}_2 &= (\sin \theta_2, 0, \cos \theta_2), \\ \hat{r}_3 &= (\sin \theta_3 \cos \phi_3, \sin \theta_3 \sin \phi_3, \cos \theta_3), \\ \hat{r}_4 &= (-\sin \theta_4 \cos \phi_4, -\sin \theta_4 \sin \phi_4, -\cos \theta_4). \end{aligned} \quad (11)$$

When  $0 < \phi_3 < \pi$ , the closure condition requires  $0 < \phi_4 < \phi_3$  and  $0 < \theta_4 < \bar{\theta}(\phi_4)$ , where

$$\bar{\theta}(\phi_4) = \text{arccot} \left( \cot \theta_2 \cos \phi_4 + \frac{\cot \theta_3 - \cot \theta_2 \cos \phi_3}{\sin \phi_3} \sin \phi_4 \right) \quad (12)$$

is determined by the intersection of plane  $C\hat{r}_4\hat{z}$   $[(\sin \phi_4)x - (\cos \phi_4)y = 0]$  and plane  $C\hat{r}_2\hat{r}_3$   $[(\cot \theta_2)x + (\sin \phi_3)^{-1}(\cot \theta_3 - \cot \theta_2 \cos \phi_3)y - z = 0]$ . Here the range of the arccotangent function is limited to  $(0, \pi)$ , as the case  $\pi < \phi_3 < 2\pi$  is just a reflection of the case  $0 < \phi_3 < \pi$  over the  $C\hat{x}\hat{z}$  plane. Therefore, the angular integral reads

$$4\pi \int_0^\pi d\theta_2 \int_0^\pi d\theta_3 \int_0^{\bar{\theta}(\phi_4)} d\theta_4 \int_0^{2\pi} d\phi_2 \times \int_0^\pi 2d\phi_3 \int_0^{\phi_3} d\phi_4 \sin \theta_2 \sin \theta_3 \sin \theta_4 = 32\pi^4, \quad (13)$$

where the first “ $4\pi$ ” factor represents the integral over the arbitrary  $\hat{r}_1$ , while the factor of “2” in the  $\phi_3$  integral accounts for the  $\pi < \phi_3 < 2\pi$  region. A more intuitive derivation of Eq. (13) can be found in the Appendix.

With Eq. (13) in hand, the FV bubble nucleation rate at time  $t$  is

$$\Gamma_r(t) \equiv \frac{d^2 P_r}{dV dt} = 32\pi^4 v_w^9 f_{\text{fv}}(t) \int_{t_c}^t dt_1 \left( \int_{t_1}^t dt'_1 \frac{a(t_1)}{a(t'_1)} \right)^2 \Gamma(t_1) \frac{a(t_1)}{a(t)} \int_{t_c}^{t_1} dt_2 \left( \int_{t_2}^t dt'_2 \frac{a(t_2)}{a(t'_2)} \right)^2 \Gamma(t_2) \frac{a(t_2)}{a(t)} \\ \times \int_{t_c}^{t_2} dt_3 \left( \int_{t_3}^t dt'_3 \frac{a(t_3)}{a(t'_3)} \right)^2 \Gamma(t_3) \frac{a(t_3)}{a(t)} \int_{t_c}^{t_3} dt_4 \left( \int_{t_4}^t dt'_4 \frac{a(t_4)}{a(t'_4)} \right)^2 \Gamma(t_4) \frac{a(t_4)}{a(t)}, \quad (14)$$

where the integrals over the scale factors come from the integration element of the radial direction in spherical coordinates. The integral simplifies to

$$\left( \int_{t_i}^t dt'_i \frac{a(t_i)}{a(t'_i)} \right)^2 \rightarrow (t - t_i)^2, \quad (15)$$

when the scale factors can be taken as constant.

**False vacuum bubble distribution**– In the reverse time description, we can use the FV bubble nucleation rate, Eq. (14), to find the FV bubble distribution. Analogously to the TV bubble case, a FV bubble which nucleates at  $t' > t$  has a radius

$$R_r(t, t') = v_w \int_t^{t'} dt'' \frac{a(t)}{a(t'')}, \quad (16)$$

at time  $t$  (note that FV bubbles are nucleated in the future).

Since FV bubbles can only nucleate in patches of TV, the average FV bubble nucleation rate is  $\bar{\Gamma}_r(t) = (1 - f_{\text{fv}}(t))\Gamma_r(t)$ . The FV bubble size distribution is then

$$\frac{n_{\text{fv}}}{dR_r}(t) = \frac{1}{v_w} \bar{\Gamma}_r(t') \frac{a^4(t')}{a^4(t)}, \quad (17)$$

where  $t'$  is resolved using Eq. (16), reducing to  $t' = t + R_r/v_w$  in the limit of constant scale factor. Integrating Eq. (17) over  $R_r$  yields the overall FV bubble number density

$$n_{\text{fv}}(t) = \int_t^{t_e} dt' \bar{\Gamma}_r(t') \frac{a^3(t')}{a^3(t)}, \quad (18)$$

where  $t_e$  is the ending time of the FOPT, which can be effectively taken as  $+\infty$  and  $f_{\text{fv}}(t_e) = 0$ .

**Exponential nucleation**– So far our results are rather general and apply to any FOPT scenario as long as the TV nucleation rate  $\Gamma(t)$  is available. We now evaluate our results in the exponential nucleation rate approximation,

$$\Gamma(t) = \Gamma_* e^{\beta(t-t_*)}, \quad (19)$$

expanded around an arbitrary time  $t_* \in (t_c, t_e)$ , where  $\beta = -dS(t)/dt|_{t_*}$  can be treated as the inverse of the FOPT duration. This exponential approximation is

accurate if the FOPT proceeds rapidly compared to the Hubble time scale, i.e.  $\beta/H(t_*) \gg 1$ . Hence, the scale factor  $a(t)$  is approximately constant over the transition and can be neglected.

There are many motivated choices for the time  $t_*$  in the exponential case such as the nucleation time ( $n_{\text{tv}} H^{-3} = 1$ ) or TV bubble percolation time ( $f_{\text{fv}} = 0.71$ ) [68–70], etc. The exponential approximation fits numerical simulations the best when  $t_*$  is chosen to be the time at which the bubble statistics are computed. For the remnant distribution, we choose  $t_*$  to be the FV bubble percolation time, defined such that  $f_{\text{fv}}(t_*) = 0.29$  and  $I_* = -\ln(0.29) = 1.238$ .

We can explicitly solve for the FV filling fraction, Eq. (3) with

$$I(t) = \frac{8\pi v_w^3 \Gamma_*}{\beta^4} e^{\beta(t-t_*)} \equiv I_* e^{\beta(t-t_*)}, \quad (20)$$

where  $\beta(t_* - t_c) \gg 1$  is used. Integrating Eq. (14), the average FV bubble nucleation rate is

$$\bar{\Gamma}_r(t) \approx \frac{I_* \beta^4}{192 v_w^3} e^{4\beta(t-t_*)} e^{-I(t)} \left( 1 - e^{-I(t)} \right). \quad (21)$$

This FV nucleation rate has the necessary properties of a solution. The factors of  $f_{\text{fv}} = e^{-I}$  and  $(1 - f_{\text{fv}}) = (1 - e^{-I})$  constrain the majority of FV bubbles to nucleate during the phase transition,  $t_c < t < t_e$ , and the factor of  $e^{4\beta(t-t_*)}$  biases the FV nucleation towards later times,  $f_{\text{fv}} \ll 1$ , which is to be expected of collapsing FV remnants. By using Eq. (17), the FV bubble distribution is found to be

$$\frac{dn_{\text{fv}}}{dR_r}(t_*) \sim \frac{1}{v_w} \Gamma_r(t_* + R/v_w) \\ = \frac{I_*^4 \beta^4}{192 v_w^3} e^{4\beta R_r/v_w} e^{-I_* e^{\beta R_r/v_w}} \left( 1 - e^{-I_* e^{\beta R_r/v_w}} \right). \quad (22)$$

**False vacuum bubble normalization**– We determine the approximate shape of the FV bubbles by normalizing the total volume contained in the FV bubbles to the filling fraction  $f_{\text{fv}}$  at the remnant percolation time  $t_*$ . While the projected collapse is tetrahedral, which would suggest a volume of  $8\sqrt{3}R^3$  for a regular tetrahedron, with  $R$  the inradius, the FV bubble is expected to become more rounded as additional TV walls partially cover the bubble. This mimics the effects of tension,

which is neglected in this treatment, but which tends to smooth the bubble edges. We expect FV bubbles at the percolation threshold to be roughly spherical but abnormally shaped, as depicted in Fig. 1. We therefore use the volume formula  $A(4\pi/3)R^3$ , where  $(A - 1)$  measures the departure from sphericity. Summing up the FV bubble volumes and normalizing to the FV fraction,

$$\int dR_r A \frac{4\pi R_r^3}{3} \frac{dn_{\text{fv}}}{dR_r}(t_*) = 0.29, \quad (23)$$

yields  $A = 1.15$ . This suggests that the FV bubbles/remnants are approximately spherical but with a non-negligible deviation. From another point of view, the factor  $A = 1.15$  is the required normalization for the formalism to be self-consistent. Although overlap between adjacent FV bubbles is ignored here, the volume  $V \approx 1.15(4\pi/3)R^3$  is the average volume that effectively “belongs” to each collapsing remnant of size  $R$  at the percolation time.

Note that the value of the FV percolation chosen here,  $f_{\text{fv}} = 0.29$ , is strictly valid only for spherical bubbles of equal size. Since the FV bubble distribution is not monochromatic, nor are they spherical, the exact percolation threshold would have to be determined by a numerical simulation. We do not expect the threshold to deviate significantly from  $f_{\text{fv}} = 0.29$ .

**Application to Primordial Black Holes**— As a concrete example, we apply our method to the Fermi-ball/PBH formation scenario proposed in Refs. [19, 34] and subsequently studied in Refs. [21, 35, 36]. During the FOPT, an asymmetric population of dark fermions  $\chi$ - $\bar{\chi}$  is trapped between the expanding TV bubble walls into the collapsing FV remnants due to a large mass differential for  $\chi$  in the two phases. As the remnants shrink, the fermions and anti-fermions annihilate, leaving only the asymmetrical portion supported by degeneracy pressure. The total number of  $\chi$  fermions trapped in a remnant with size  $R_*$  at the FV percolation time  $t_*$  is [19, 34]

$$Q_{\text{FB}} = \frac{\eta_\chi s(t_*)}{f_{\text{fv}}(t_*)} A \frac{4\pi R_*^3}{3}, \quad (24)$$

where  $\eta_\chi = (n_\chi - n_{\bar{\chi}})/s$  is the  $\chi$ -asymmetry with  $s$  the entropy density.

Since the Fermi-ball/PBH mass  $M_{\text{PBH}} \propto Q_{\text{FB}}$  [19], the distribution of  $R_*$  is key to deriving the Fermi-ball/PBH mass profile. Lacking methods to compute the  $R_*$  distribution, Refs. [19, 34] estimated the average size to be

$$R_* \sim \left( \frac{3v_w}{4\pi A \Gamma_*} \right)^{1/4} = 1.43 \frac{v_w}{\beta}, \quad (25)$$

resulting in a monochromatic Fermi-ball/PBH mass distribution. With the technique developed in this *Letter*,

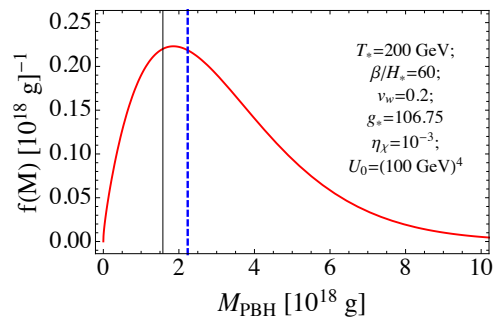


FIG. 3. A benchmark  $f(M_{\text{PBH}})$  distribution (red curve) for the Fermi-ball/PBH formation scenario of Ref. [34], where  $f$  is the PBH mass distribution probability function. The FOPT parameters are shown in the figure, with  $U_0$  the energy density difference between the TV and FV. The vertical black thin line and blue dashed line represent  $\langle M_{\text{PBH}} \rangle$  from our work and the estimate of  $M_{\text{PBH}}$  from Ref. [34], respectively.

we are able to derive the  $R_*$  distribution using Eq. (22), and obtain

$$\langle R \rangle_* = \int dR_r R_r \frac{dn_{\text{fv}}}{dR_r}(t_*) = 1.12 \frac{v_w}{\beta}. \quad (26)$$

Although this seems quite close to the estimated value, a continuous  $R_*$  distribution results in an extended Fermi-ball/PBH mass profile, which greatly impacts experimental constraints [71]. In Fig. 3, we compute an example PBH distribution at present time which comprises all of dark matter and lie within the PBH mass window,  $10^{17} \text{ g} < M < 10^{23} \text{ g}$ , where there are no reliable bounds on PBH dark matter [72].

**Discussion**— In our derivation of the FV bubble nucleation rate Eq. (14), we made a few simplifying assumptions. First, the walls were assumed to be infinitesimally thin and the wall velocity constant. TV bubble mergers can alter the effective location of the TV wall nucleation and expansion direction. Furthermore, surface tension tends to shape the collapsing remnants to be more spherical, whereas the collapsing remnant is treated as tetrahedral with four planar walls. All of these effects are exacerbated near the end of the phase transition when TV bubbles inevitably merge, surface tension becomes more prominent as the surface area to volume ratio increases, and particle trapping may stop or slow the collapse.

We resolve these issues by interpreting the method and formalism of computing  $\Gamma_r(t)$  developed in this *Letter* as a projected description of the FOPT rather than a physical description. In other words, beyond the remnant percolation time  $t_*$  at which we evaluate Eq. (22), the future evolution of the FOPT is irrelevant to the remnant statistics evaluated at  $t_*$ . Causally, the remnant size distribution and number density at  $t_*$  cannot be affected



by events at later times  $t > t_*$ . Thus, the remnant statistics at the remnant percolation time depend only on the history of the FOPT up to the that time, before which these four assumptions are only mildly violated. The calculated observables will be the same whether, in the later stages of the transition, our idealized collapse scenario is applied or a more physical scenario with surface tension effects is used instead. Hence, the projection interpretation is that our formalism essentially traces the walls of the collapsing remnants forward past time  $t_*$  to find the collapse point, in order to then trace the collapse backwards in the reverse time description and infer the size of the remnant at time  $t_*$ .

We offer an analogy: the shadow of a falling apple can be used to infer its instantaneous position. Whether or not the apple eventually lands directly on its shadow, is perturbed by a gust of wind, or drops on an unwitting head, is immaterial to the determination of its instantaneous position. Likewise, whether the remnant eventually collapses spherically or is stopped by degeneracy pressure is irrelevant to its size distribution at remnant percolation. Therefore, in the derivation of the remnant distribution, our tetrahedral collapse model is more appropriate than a physically realistic spherical collapse model because the shadow (or projection) of the collapsing walls is tetrahedral and not spherical.

In summary, we have performed the first analytical calculation of the FV remnant distribution and evolution in FOPTs. By identifying the center of a collapsing remnant as a FV bubble nucleation in reverse, the established TV bubble nucleation formalism can be adapted to derive remnant statistics. Our results provide a more sophisticated treatment of FOPT remnants than previously available, and are directly applicable to many new physics mechanisms involving trapped particles [14–21, 32–36, 64]. The novel formalism developed in this *Letter* can be readily generalized and applied outside the cosmological context.

**Acknowledgments.**— We thank Sunghoon Jung, Hyung Do Kim, Taehun Kim, and Howard Chen for useful discussions. The work of P.L. was supported by the Grant Korea NRF-2019R1C1C1010050. K.P.X. is supported by the University of Nebraska-Lincoln. The work of K.K. is supported by Grant Korea NRF-2019R1C1CC1010050, 2019R1A6A1A10073437.

---

\* [philip11@gmail.com](mailto:philip11@gmail.com)

† [kawana@snu.ac.kr](mailto:kawana@snu.ac.kr)

‡ [kepan.xie@unl.edu](mailto:kepan.xie@unl.edu)

[1] Y. Lu, Y. Lu, J. Ma, J. Li, X. Huang, Q. Jia, D. Ma, M. Liu, H. Zhang, X. Yu, et al., bioRxiv (2021), URL <https://www.biorxiv.org/content/early/2021/04/20/2021.04.15.439963>.

- [2] A. Narayanan, A. B. Meriin, M. Y. Sherman, and I. I. Cissé, bioRxiv (2017), URL <https://www.biorxiv.org/content/early/2017/06/19/148395>.
- [3] M. Blume, *Physical Review* **141**, 517 (1966).
- [4] S. Sachdev, *Quantum Phase Transitions* (2011).
- [5] K. Sato, *Mon. Not. Roy. Astron. Soc.* **195**, 467 (1981).
- [6] V. A. Kuzmin, V. A. Rubakov, and M. E. Shaposhnikov, *Phys. Lett. B* **155**, 36 (1985).
- [7] M. Joyce, T. Prokopec, and N. Turok, *Phys. Rev. D* **53**, 2958 (1996), hep-ph/9410282.
- [8] M. Joyce, T. Prokopec, and N. Turok, *Phys. Rev. Lett.* **75**, 1695 (1995), [Erratum: *Phys. Rev. Lett.* **75**, 3375 (1995)], hep-ph/9408339.
- [9] A. G. Cohen, D. B. Kaplan, and A. E. Nelson, *Ann. Rev. Nucl. Part. Sci.* **43**, 27 (1993), hep-ph/9302210.
- [10] D. E. Morrissey and M. J. Ramsey-Musolf, *New J. Phys.* **14**, 125003 (2012), 1206.2942.
- [11] M. J. Baker and J. Kopp, *Phys. Rev. Lett.* **119**, 061801 (2017), 1608.07578.
- [12] M. J. Baker, J. Kopp, and A. J. Long, *Phys. Rev. Lett.* **125**, 151102 (2020), 1912.02830.
- [13] D. Chway, T. H. Jung, and C. S. Shin, *Phys. Rev. D* **101**, 095019 (2020), 1912.04238.
- [14] E. Witten, *Phys. Rev. D* **30**, 272 (1984).
- [15] E. Krylov, A. Levin, and V. Rubakov, *Phys. Rev. D* **87**, 083528 (2013), 1301.0354.
- [16] F. P. Huang and C. S. Li, *Phys. Rev. D* **96**, 095028 (2017), 1709.09691.
- [17] Y. Bai and A. J. Long, *JHEP* **06**, 072 (2018), 1804.10249.
- [18] Y. Bai, A. J. Long, and S. Lu, *Phys. Rev. D* **99**, 055047 (2019), 1810.04360.
- [19] J.-P. Hong, S. Jung, and K.-P. Xie, *Phys. Rev. D* **102**, 075028 (2020), 2008.04430.
- [20] P. Asadi, E. D. Kramer, E. Kuflik, G. W. Ridgway, T. R. Slatyer, and J. Smirnov, *Phys. Rev. Lett.* **127**, 211101 (2021), 2103.09822.
- [21] D. Marfatia and P.-Y. Tseng, *JHEP* **11**, 068 (2021), 2107.00859.
- [22] M. Crawford and D. N. Schramm, *Nature* **298**, 538 (1982).
- [23] S. W. Hawking, I. G. Moss, and J. M. Stewart, *Phys. Rev. D* **26**, 2681 (1982).
- [24] D. La and P. J. Steinhardt, *Phys. Lett. B* **220**, 375 (1989).
- [25] I. G. Moss, *Phys. Rev. D* **50**, 676 (1994).
- [26] R. Konoplich, S. Rubin, A. Sakharov, and M. Y. Khlopov, *Astronomy Letters* **24**, 413 (1998).
- [27] R. V. Konoplich, S. G. Rubin, A. S. Sakharov, and M. Y. Khlopov, *Phys. Atom. Nucl.* **62**, 1593 (1999).
- [28] H. Kodama, M. Sasaki, and K. Sato, *Prog. Theor. Phys.* **68**, 1979 (1982).
- [29] M. Lewicki and V. Vaskonen, *Phys. Dark Univ.* **30**, 100672 (2020), 1912.00997.
- [30] A. Kusenko, M. Sasaki, S. Sugiyama, M. Takada, V. Takhistov, and E. Vitagliano, *Phys. Rev. Lett.* **125**, 181304 (2020), 2001.09160.
- [31] C. Gross, G. Landini, A. Strumia, and D. Teresi, *JHEP* **09**, 033 (2021), 2105.02840.
- [32] M. J. Baker, M. Breitbach, J. Kopp, and L. Mitnacht (2021), 2105.07481.
- [33] M. J. Baker, M. Breitbach, J. Kopp, and L. Mitnacht (2021), 2110.00005.
- [34] K. Kawana and K.-P. Xie, *Phys. Lett. B* **824**, 136791 (2022), 2106.00111.

- [35] D. Marfatia and P.-Y. Tseng (2021), 2112.14588.
- [36] P. Huang and K.-P. Xie (2022), 2201.07243.
- [37] J. Liu, L. Bian, R.-G. Cai, Z.-K. Guo, and S.-J. Wang (2021), 2106.05637.
- [38] H. Davoudiasl, P. B. Denton, and J. Gehrlein (2021), 2109.01678.
- [39] T. H. Jung and T. Okui (2021), 2110.04271.
- [40] K. Hashino, S. Kanemura, and T. Takahashi (2021), 2111.13099.
- [41] D. N. Maeso, L. Marzola, M. Raidal, V. Vaskonen, and H. Veermäe (2021), 2112.01505.
- [42] X. Xue et al., Phys. Rev. Lett. **127**, 251303 (2021), 2110.03096.
- [43] Z. Arzoumanian et al. (NANOGrav), Astrophys. J. Lett. **905**, L34 (2020), 2009.04496.
- [44] A. Romero, K. Martinovic, T. A. Callister, H.-K. Guo, M. Martínez, M. Sakellariadou, F.-W. Yang, and Y. Zhao, Phys. Rev. Lett. **126**, 151301 (2021), 2102.01714.
- [45] C. Caprini et al., JCAP **04**, 001 (2016), 1512.06239.
- [46] C. Caprini et al., JCAP **03**, 024 (2020), 1910.13125.
- [47] Z.-C. Liang, Y.-M. Hu, Y. Jiang, J. Cheng, J.-d. Zhang, and J. Mei, Phys. Rev. D **105**, 022001 (2022), 2107.08643.
- [48] C. J. Hogan, Mon. Not. Roy. Astron. Soc. **218**, 629 (1986).
- [49] M. Maggiore, Phys. Rept. **331**, 283 (2000), gr-qc/9909001.
- [50] K. Kawana (2022), 2201.00560.
- [51] C. G. Callan, Jr. and S. R. Coleman, Phys. Rev. D **16**, 1762 (1977).
- [52] A. H. Guth and S. H. H. Tye, Phys. Rev. Lett. **44**, 631 (1980), [Erratum: Phys.Rev.Lett. 44, 963 (1980)].
- [53] A. H. Guth and E. J. Weinberg, Phys. Rev. D **23**, 876 (1981).
- [54] I. Affleck, Phys. Rev. Lett. **46**, 388 (1981).
- [55] M. Dine, R. G. Leigh, P. Y. Huet, A. D. Linde, and D. A. Linde, Phys. Rev. D **46**, 550 (1992), hep-ph/9203203.
- [56] J. R. Espinosa, T. Konstandin, J. M. No, and G. Servant, JCAP **06**, 028 (2010), 1004.4187.
- [57] A. Megevand and S. Ramirez, Nucl. Phys. B **919**, 74 (2017), 1611.05853.
- [58] J. Ellis, M. Lewicki, and J. M. No, JCAP **04**, 003 (2019), 1809.08242.
- [59] X. Wang, F. P. Huang, and X. Zhang, JCAP **05**, 045 (2020), 2003.08892.
- [60] D. Bodeker and G. D. Moore, JCAP **05**, 009 (2009), 0903.4099.
- [61] D. Bodeker and G. D. Moore, JCAP **05**, 025 (2017), 1703.08215.
- [62] S. Höche, J. Kozaczuk, A. J. Long, J. Turner, and Y. Wang, JCAP **03**, 009 (2021), 2007.10343.
- [63] Y. Gouttenoire, R. Jinno, and F. Sala (2021), 2112.07686.
- [64] J. Arakawa, A. Rajaraman, and T. M. P. Tait (2021), 2109.13941.
- [65] A. D. Linde, Nucl. Phys. B **216**, 421 (1983), [Erratum: Nucl.Phys.B 223, 544 (1983)].
- [66] S. R. Coleman, Phys. Rev. D **15**, 2929 (1977), [Erratum: Phys.Rev.D 16, 1248 (1977)].
- [67] M. D. Rintoul and S. Torquato, Journal of physics a: mathematical and general **30**, L585 (1997).
- [68] D. F. Holcomb and J. J. Rehr, Phys. Rev. **183**, 773 (1969), URL <https://link.aps.org/doi/10.1103/PhysRev.183.773>.
- [69] M. D. Rintoul and S. Torquato, Journal of Physics A: Mathematical and General **30**, L585 (1997), URL <https://doi.org/10.1088/0305-4470/30/16/005>.
- [70] M. Li, H. Chen, and J. Lin, Computer Methods in Applied Mechanics and Engineering **361**, 112815 (2020), ISSN 0045-7825, URL <https://www.sciencedirect.com/science/article/pii/S0045782519307078>.
- [71] A. M. Green and B. J. Kavanagh, J. Phys. G **48**, 043001 (2021), 2007.10722.
- [72] B. Carr, K. Kohri, Y. Sendouda, and J. Yokoyama, Rept. Prog. Phys. **84**, 116902 (2021), 2002.12778.

## Appendix - Angular Contribution

We present an alternative derivation of the angular factor in three dimensions (Eq. (13)). Here we order the walls and set up the spherical coordinate system in the same manner as in the main body of the text. Requiring  $-\hat{\mathbf{r}}_4$  to be in the solid angle established by  $\hat{\mathbf{r}}_1, \hat{\mathbf{r}}_2$ , and  $\hat{\mathbf{r}}_3$  results in the two conditions

$$\pi \leq \phi_4 \leq \pi + \phi_3, \quad (27)$$

and

$$\max(\theta_2, \theta_3, \theta_4) \geq \pi - \min(\theta_2, \theta_3, \theta_4). \quad (28)$$

The  $\phi$  condition can be understood as the requirement that walls 2, 3 and 4 form a triangle in the plane of wall 1, and so is analogous to the two-dimensional case (Eq. (9)). The  $\theta$  condition can be interpreted as the need to form a closed tetrahedron in the  $\hat{z}$  direction. To understand this condition, first sort the angles  $\theta_2, \theta_3, \theta_4 \rightarrow \theta_l \leq \theta_m \leq \theta_h$ . Take the limiting case where wall  $h$  is arranged opposite of wall  $l$ , so that the corresponding azimuthal angles satisfy  $\phi_h = \pi + \phi_l$ . We see that the closure requirement is satisfied if  $\pi - \theta_l \leq \theta_h \leq \pi$ , where at the lower bound wall  $h$  lies directly opposite of wall  $l$  and at the upper bound, wall  $h$  is directly opposite wall 1.

The, the  $\phi$  contribution to the three-dimension probability integral is

$$\int_0^{2\pi} d\phi_1 \int_0^{2\pi} d\phi_2 \int_0^\pi 2d\phi_3 \int_\pi^{\pi+\phi_3} d\phi_4 = 4\pi^4, \quad (29)$$

and the  $\theta$  contribution is

$$\begin{aligned} & \int_0^\pi d\theta_1 \sin \theta_1 \, 3! \int_0^\pi d\theta_l \sin \theta_l \int_{\max(\pi-\theta_l, \theta_l)}^\pi d\theta_h \sin \theta_h \\ & \times \int_{\theta_l}^{\theta_h} d\theta_m \sin \theta_m = 8. \end{aligned} \quad (30)$$

The combinatoric factor of  $3!$  comes from the sorting of  $\theta_2, \theta_3$ , and  $\theta_4$  into the low, medium, and high angles. As in Eq. (13), the combined angular contribution is  $32\pi^4$ .